doi:10.15625/2525-2518/18507



Green synthesis of nanostructured 1T/2H-MoS₂ hybrid phase with polyol solvents and microwave heating

Nguyen Thi Minh Nguyet^{1, 2, *}, Vuong Vinh Dat^{2, 3}, Nguyen Huu Huy Phuc^{2, 3}, Le Van Thang^{1, 2}

¹VNU-HCM Key Laboratory for Material Technologies, Ho Chi Minh City University of Technology (HCMUT), 268 Ly Thuong Kiet, Dien Hong Ward, Ho Chi Minh City, Viet Nam

²Vietnam National University Ho Chi Minh City, Linh Xuan Ward, Ho Chi Minh City, Viet Nam

³Faculty of Materials Technology, Ho Chi Minh City University of Technology (HCMUT),

268 Ly Thuong Kiet Street, Dien Hong Ward, Ho Chi Minh City, Viet Nam

*Email: minhnguyet@hcmut.edu.vn

Received: 12 July 2023; Accepted for publication: 28 March 2024

Abstract. Green synthesis approaches have attracted much attention in recent years since they address sustainability-related issues better than conventional synthesis methods. New research fields in green nanoscience are being developed as a result of the incorporation of green chemistry principles into nanoscience. In this paper, the successful microwave-assisted green synthesis of MoS₂ nanoparticles in a single pot using polyol solvents such as ethylene glycol and glycerol is demonstrated. The coexistence of 1T and 2H phases in MoS₂ nanomaterials was determined using advanced techniques such as XRD, Raman, XPS, and TEM images. The highest 1T proportion obtained was 84.5 % when compared to the 2H phase. The reaction mechanism and the phase transition between 1T and 2H are described and illustrated. The role of polyol solvents in the practical synthesis of nano MoS₂ under microwave heating is also evaluated and explained. Due to the ability of the metallic 1T phase to enhance electrical conductivity, it is believed that hybrid nanostructures exhibit superior electrochemical performance for energy storage and conversion applications.

Keywords: nano MoS₂, hybrid phase 1T/2H-MoS₂, polyol solvents, microwave synthesis, green chemistry *Classification numbers*: 2.4.2, 2.4.4, 5.2.1

1. INTRODUCTION

The metallic 1T phase of MoS_2 nanomaterials shows enhanced electron transport, ion diffusion, and catalytic activity compared to the semiconducting 2H phase, owing to its larger interlayer spacing and higher conductivity [2 - 12]. In 1T/2H mixed-phase heterostructures, partial phase transformation reduces the kinetic barrier and promotes charge transfer, increasing active sites and improving catalytic and electrochemical performance [6, 12 - 15]. These hybrids exhibit high specific capacitance, excellent rate capability, and long-term durability, making them ideal for supercapacitor electrodes [7, 16].

Environmentally friendly synthesis approaches-particularly green methods using microwave heating-are gaining attention for their simplicity, energy efficiency, and

reproducibility [17 - 19]. Microwave heating rapidly generates heat at the interfaces of polar solvents, enhancing reaction rates and reducing solvent use [20 - 23]. The choice of solvent is critical: polyols such as ethylene glycol (EG) and glycerol (G) are widely used due to their high boiling points, suitable viscosity, and ability to support nanoparticle formation under microwave irradiation [24 - 26].

This study employs a green, microwave-assisted approach to synthesize $1T/2H-MoS_2$ nanostructures using polyol solvents. It investigates their structure, formation mechanism, and electrochemical potential for energy storage applications.

2. MATERIALS AND METHODS

To synthesize MoS₂ nanostructures, 1.24 g of ammonium heptamolybdate tetrahydrate ((NH₄)₆Mo₇O₂₄·4H₂O) and 2.28 g of thiourea (CSN₂H₄) were dissolved in 60 mL of solvent—either ethylene glycol (EG), glycerol (G), or a 1:1 EG/G mixture—and stirred at 60 °C for 30 min. The solution was then microwaved at 240 W for 15 min, reaching the solvents' boiling points. After cooling, black precipitates were washed with ethanol, centrifuged, and vacuum dried at 80 °C for 5 h. The samples were labeled S1 (EG), S2 (EG+G), and S3 (G).

Structural analysis was performed via XRD (Bruker D8 Advance, Cu K α , 5°–80°, 1°/min, step 0.0194°) and Raman spectroscopy (Labram HR VIS, 632.8 nm, 1 mW, 300 lines/mm grating). TEM images were acquired using JEOL-TEM-1400 at 200 kV (bright field mode). XPS analysis (ESCALAB 250, Al K α) was conducted to assess surface composition; binding energies were calibrated to C 1s at 284.6 eV, with constant FWHM for doublets.

3. RESULTS AND DISCUSSION

X-ray diffraction (XRD) analysis is a commonly used technique to determine the crystal structure and size, as well as the crystalline phase and purity of a crystal. During the microwave irradiation process, intercalation and heat treatment can significantly impact the crystal structure of the host materials, resulting in a phase transition from semiconducting (2H) to metallic (1T), as seen in the XRD pattern presented in Figure 1.

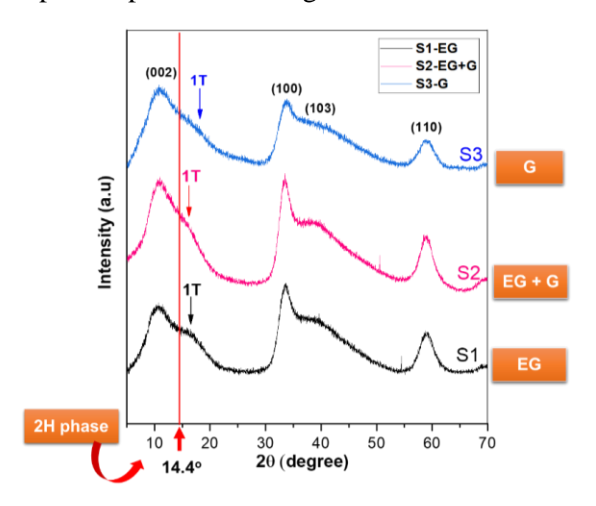


Figure 1. XRD patterns of S1-EG, S2-EG+G, and S3-G.

To determine the XRD spectrum of mixed-phase 1T/2H-MoS₂, a comparison with the XRD

spectrum of bulk 2H-MoS₂ is necessary [1, 27]. Figure 1 shows the XRD patterns of the three samples (S1-EG, S2-EG+G, and S3-G). All samples exhibit XRD peaks at 31.9°, 43.3°, and 56.8°, which correspond to the (100), (103), and (110) planes of MoS₂, respectively. However, the characteristic peak of the (002) plane of 2H-MoS₂ at ~14.41° is absent and instead exhibits peak splitting at lower and higher 2 θ angles (red dashed rectangle in Figure 1). This disordered structure matches the previously reported ammoniated 1T-MoS₂ [7], indicating the formation of a 1T/2H-MoS₂ hybrid phase. The large interlayer spacing of the as-prepared MoS₂ in those of S1-EG (2 θ ~ 10.6°), S2-EG+G (2 θ ~ 10.9°), S3-G (2 θ ~ 10.9°) is attributed to the high content of 1T-MoS₂ in these samples [28].

Figure 2A displays the Raman spectra of S1-EG, S2-EG+G, and S3-G, which were synthesized using various solvents such as EG, EG+G, and glycerol (G). Table 1 summarizes the detected vibrations in all three samples. A more detailed view of the vibrational modes is presented in Figure 2C. The observed strong peaks at 141, 190, 230, and 331 cm⁻¹, which correspond to the stretching vibration of Mo–Mo and the phonon mode of 1T-MoS₂, indicate the presence of 1T-MoS₂ in all samples [1, 28, 29]. The A_{1g} to J_1 intensity ratio in a spatially resolved Raman spectra of MoS₂ can be utilized to determine the phase content, as it is inversely proportional to the amount of 1T phase present. In S1-EG, S2-EG+G, and S3-G, the J_1 peak is visible, but the A_{1g}/J_1 value is extremely low and cannot be seen in Figure 2B when zoomed in, indicating a high 1T phase content. The increase in the A_{1g}/J_1 value indicates a decrease in the 1T phase content and the formation of a mixed phase of 1T/2H [30]. This explains the absence of A_{1g} peaks in the Raman spectra of samples S1-EG, S2-EG+G, and S3-G, as shown in Figure 2B. Additionally, the low crystallinity and lack of 2H phase in the MoS₂ material may account for the significant reduction in the intensity of typical E_{2g}^1 and A_{1g} peaks over 1T/2H-MoS₂ in S1-EG, S2-EG+G, and S3-G [1, 13].

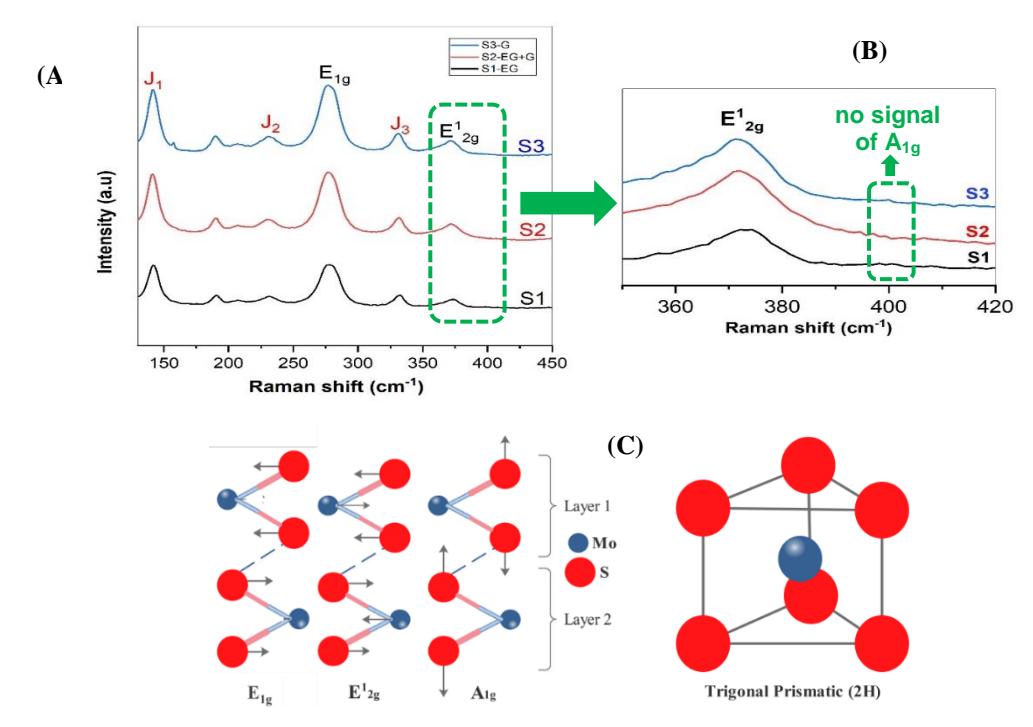


Figure 2. (A) Raman spectra of S1-EG, S2-EG+G, S3-G; (B) Maginified Raman signals of green area from Figure 2A; and (C) Symmetric displacement of Mo and S atoms in E_{1g} , E_{2g}^1 and A_{1g} vibrational modes.

Table 1. Summary of vibration modes (position peaks) in S1, S2, and S3 (cm⁻¹).

Sample	J_1	Phonon mode	J_2	E_{1g}	J_3	E^1_{2g}	A_{1g}
S1-EG	~141.6	~ 190	~230	~278	~331	~372	-
S2-EG+G	~141.5	~ 190	~230	~278	~331	~372	-
S3-G	~141.9	~ 190	~230	~278	~331	~372	-

Table 2. 1T and 2H phase proportions in MoS_2 nanomaterials synthesized in different polyol solvents.

PHASE	PHASE FRACTION					
	S1-EG	S2-EG+G	S3-G			
2Н	15.5 %	19.8 %	20.8 %			
1T	84.5 %	80.2 %	71.2 %			

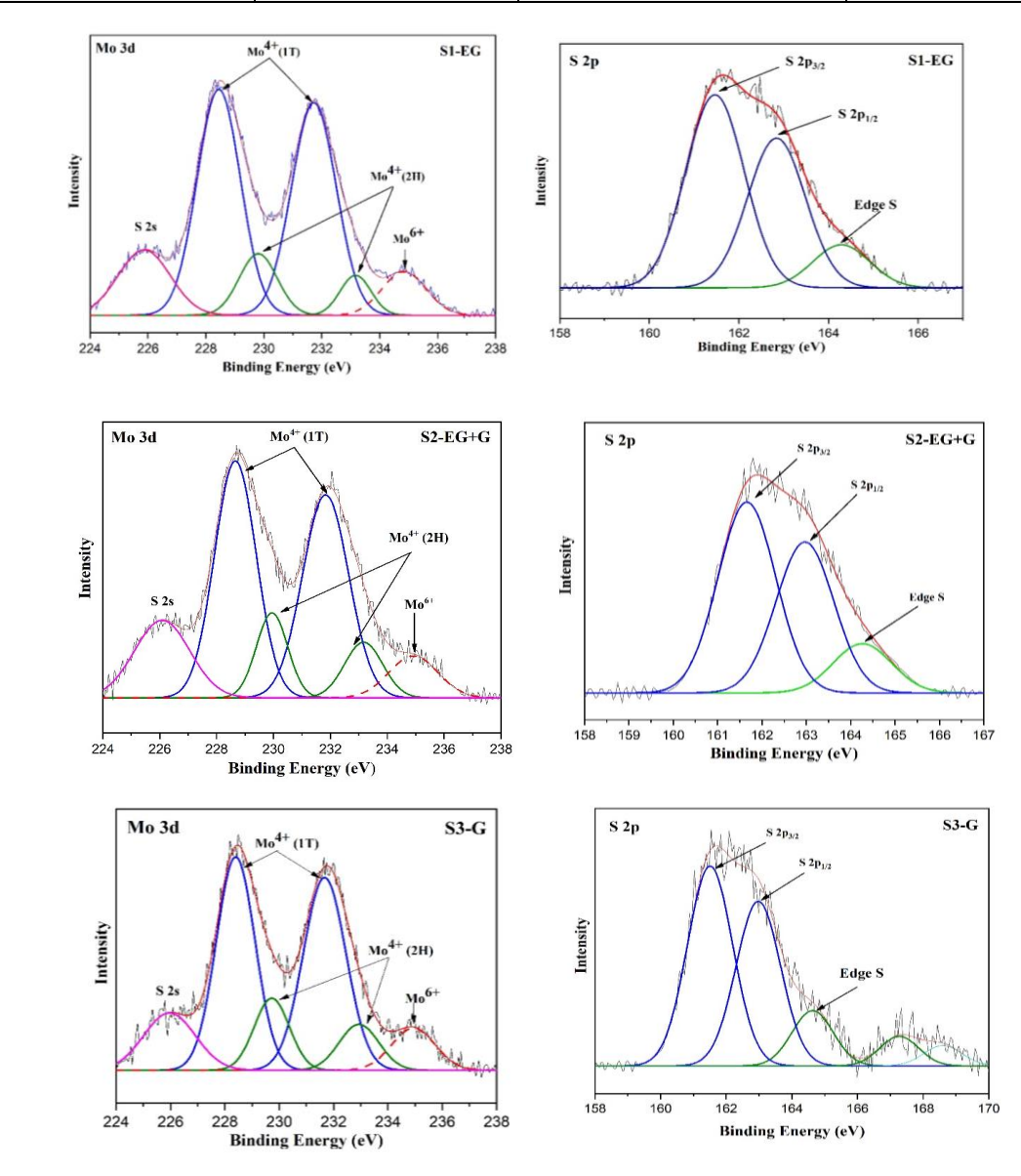


Figure 3. Mo 3d and S 2s XPS spectra of $1T/2H-MoS_2$ in S1-EG, S2-EG+G, and S3-G.

XPS spectra (Figure 3) confirm the formation of MoS₂ with signals for both 1T and 2H phases, and trace MoO₃. The Mo 3d region shows characteristic doublets for Mo⁴⁺: ~228.4/231.7 eV for 1T-MoS₂ and ~229.8/233.2 eV for 2H-MoS₂ [1, 3, 7, 8, 31 - 36]. These binding energies shift relative to elemental Mo (228/231.1 eV), reflecting phase-dependent electronic environments The ~3.2 eV splitting and 3:2 intensity ratio between 3d₅/₂ and 3d₃/₂ align with expected Mo oxidation states [37]. In 1T-MoS₂, the lower binding energies (~1.3 eV downshift from 2H) indicate higher electron density, consistent with earlier studies [29, 34, 38, 39]. S 2p spectra show peaks at ~161.5 and 162.8 eV for S²⁻, also shifted in 1T-MoS₂ due to electron-rich Mo–S bonds [40, 41]. A minor peak near 225.9 eV (S 2s) supports Mo–S bonding, while a peak around 235 eV suggests Mo⁶⁺ in MoO₃, likely from surface oxidation [38].

The relative concentration of the 1T and 2H phases in various solvents was calculated using XPS as the ratio between the Mo 3d peak areas. Each phase's fraction was calculated following the equation (1) below and then summarized in Table 2 [42]. All the MoS₂ products comprise both phases - 1T and 2H - but their compositions vary depending on the solvents (reaction temperatures). Notably, 1T phase proportion was reduced when increasing the reaction temperatures ($T_{EG} < T_{(EG+G)} < T_G$) [43]. The low temperature of MoS₂ synthesized in ethylene glycol (EG) enabled such a rich composition of the 1T-phase, as 84.5 % as calculated in Table 2 with added mechanical and thermal stability due to co-existence with the 2H-phase. Because of the presence of a highly conductive 1T phase rather than a 2H phase, these hybrid materials have the potential to improve the electrochemical properties of batteries or capacitors.

Fraction of 2H phase =
$$\frac{2H\left(3d_{5/2}\right) + 2H\left(3d_{3/2}\right)}{2H\left(3d_{5/2}\right) + 2H\left(3d_{3/2}\right) + 1T\left(3d_{5/2}\right) + 1T\left(3d_{3/2}\right)} \times 100\% \ \ (1) \ [42]$$

High-resolution TEM (HRTEM) was performed to visualize the 1T/2H crystal surface structures with lattice fringes (Figure 4). The enlarged red rectangle in Figure 4A, depicted in Figures 4B and 4C, reveals the trigonal lattice area of the 1T phase and the honeycomb lattice area of the trigonal prismatic coordination in the 2H phase. As depicted in Figure 4D, the interlayer distances were measured to be 0.236 nm, which is given to the d spacing of the (100) planes of the 1T phase MoS_2 [44].

Figure 5 illustrates the formation of diverse morphologies in the MoS₂ materials. When comparing the nanoparticle morphology of the S1-EG and S3-G samples, the TEM images of the S2-EG+G sample reveal the presence of numerous nanoflake wrinkles. These wrinkles are agglomerates or aggregates composed of homogeneous MoS₂ particles or flakes. The particle boundaries are more distinct in S3-G compared to S1-EG and S2-EG+G. In S1-EG and S2-EG+G, the flakes exhibit corrugation, indicating the flexible and ultrathin nature of the material.

The integration of TEM images with XRD, Raman, and XPS data offers compelling evidence that MoS₂ materials have been successfully synthesized at the nanoscale, exhibiting diverse morphologies. Remarkably, the TEM images reveal variations in the size and shape of metal sulfide nanoparticles, even when employing the same microwave synthesis route. These findings suggest that microwave irradiation can selectively influence the nucleation and growth rates of distinct compounds.

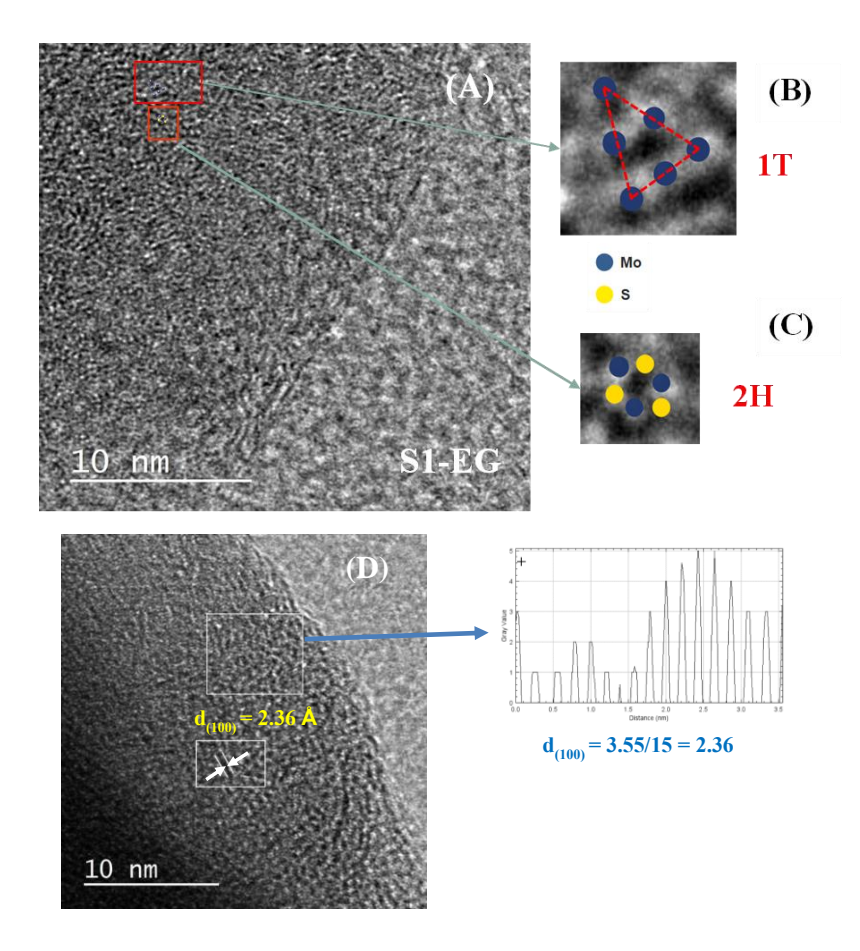
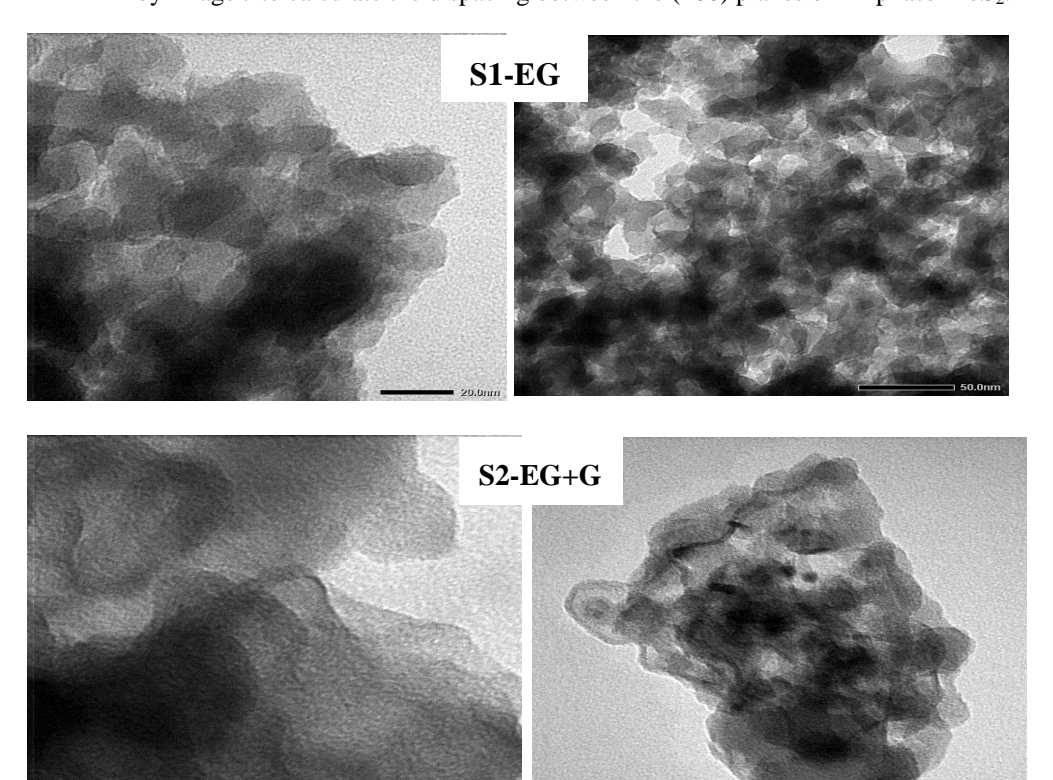


Figure 4. (A) HRTEM images of S1-EG; (B) Image of the region enclosed by the redrectangle of (A) and schematic structure of the unit cells of the 1T phase; (C) Image of the region enclosed by the red rectangle in (A) and schematic structure of the unit cells of the 2H phase; (D) Measurement of interlayer distances by Image J to calculate the d spacing between the (100) planes of 1T phase MoS₂.



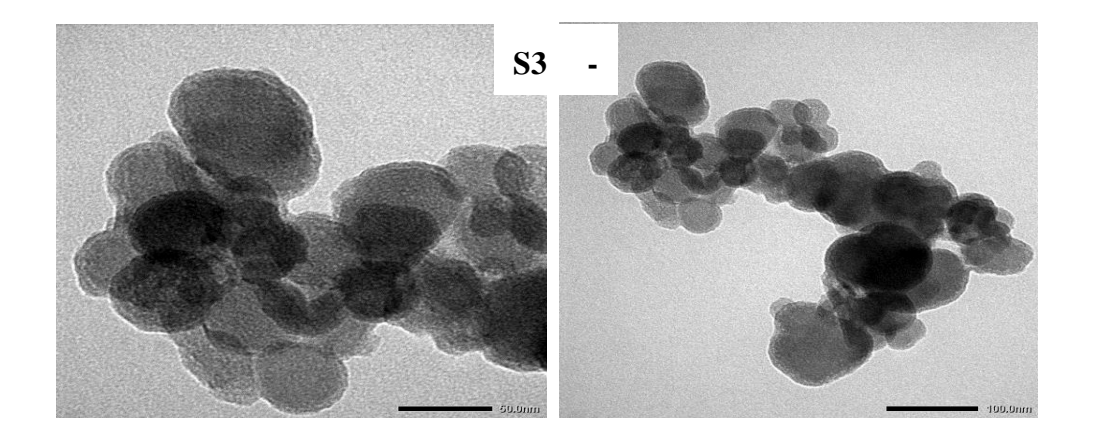


Figure 5. TEM images of 1T/2H-MoS₂ in S1-EG, S2-EG+G and S3-G.

Explaining the mechanism for synthesis reaction and proposing the structure of asprepared material

The probable mechanism of the reaction of microwave heating synthesis of 1T/2H-MoS₂ nanoparticles is presented by the following steps:

(1) **Dissociation**: Two types of water are present in the precursor: structural water, which is bound chemically and is an integral part of $(NH_4)_6(Mo_7O_{24})\cdot 4H_2O$, and water present in ethylene glycol. Microwave-induced dissociation reactions of AHM and TU species in polyol solvents are likely to occur according to the following equations:

$$(NH_4)_6(Mo_7O_{24}) \cdot 4H_2O + H_2O \rightarrow [Mo_7O_{24}]^{6} + 6NH_4^+$$
 (2)

$$[Mo_7O_{24}]^{6} \rightarrow 6[MoO_4]^{2-} + Mo^{6+}$$
 (3)

$$H_2NCSNH_2 \rightarrow NH_4^+ + NCS^-$$
 (4)

$$H_2NCSNH_2 + H_2O \rightarrow 2NH_3 + CO_2 + H_2S$$
 (5)

(2) Nucleation: Initially, MoS_2 nanocrystal seeds are formed due to the reaction between AHM and thiourea. The nucleation process initiates the formation of a new crystalline entity from a solution. During the synthesis process, nanocrystal seeds grow into larger crystals and gather together to form clusters, while new crystals are continuously formed. The reactions proceed as follows:

$$MoO_4^{2-} + H_2S + 2H_2O \rightarrow MoO_2 + SO_4^{2-} + 6H^+$$
 (6)

$$MoO_2 + 2H_2S \rightarrow MoS_2 + 2H_2O \tag{7}$$

(3) Crystal growth: Initially, MoS₂ nanocrystal seeds are generated due to the reaction between AHM with thiourea. The nanocrystal seeds grow into larger crystals and cluster together throughout the synthesis process while new crystals continue to form. Mo atoms and S atoms form a chemical bond along the plane direction in a monolayer MoS₂, much stronger than the Van der Waals force between two monolayers MoS₂. As a result of the ability of MoS₂ to form stable Mo-S bonds in the plane direction, massive MoS₂ flakes can be observed in clusters

in various solutions such as EG, glycerol, and EG/G. Ammonium ions can penetrate the gap between the MoS_2 monolayers, resulting in a relatively small flake size and many bulk structures with a considerable layer distance. These bulk formations are thought to be generated by the aggregation of small MoS_2 flakes.

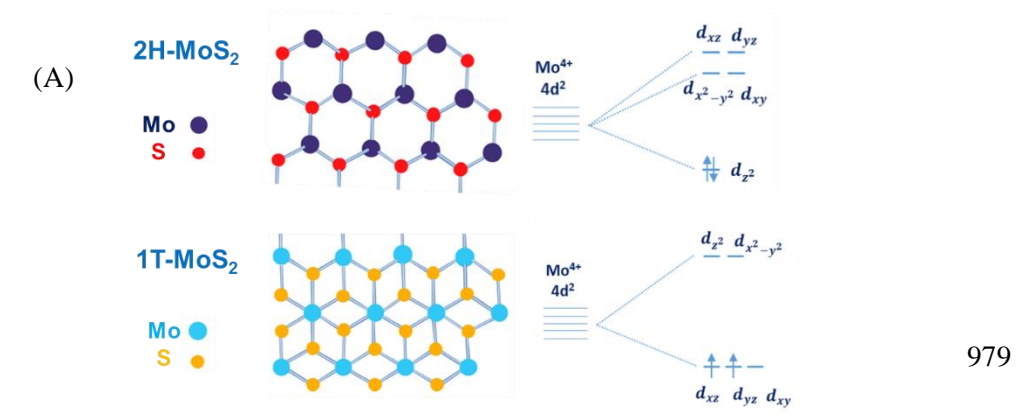
An illustrated mechanism for the growth of MoS_2 crystals involves the presence of $[Mo_7O_{24}]^{6-}$ ionic groups in a neutral solution. These groups are composed of seven octahedral $[MoO_6]$ ionic groups that contain Mo and O atoms with three different bond lengths. As NH_2CSNH_2 produces S^{2-} ions, they replace the terminal O atoms connected by the Mo–O ionic bond because the bond energy of Mo–S is higher than that of the terminal Mo–O bond [45].

Solvents play significant roles in microwave-assisted liquid-phase synthesis. Ethylene glycol (EG) and glycerol (G) have a high boiling point (>180 °C), are microwave-compatible, have an appropriate viscosity, and promote nanoparticle nucleation and development in high boiling polyols. The nucleation and growth of nanoparticles in high boiling polyols such as ethylene glycol (EG) and glycerol are the primary reasons for their use in nano MoS₂ production. The polyol acts as a solvent and a stabilizing agent, in this case, restricting particle growth while limiting particle agglomeration and aggregation [46].

Explaining the phase transitions between 1T and 2H under microwaves irradiation

2H phase formed in the first stage and then transitioned to a 1T phase via an NH_4^+ ion-induced phase transformation, similar to intercalated Li^+ [47]. The NH^{4+} ion destabilizes the trigonal-prismatic 2H- MoS_2 structure, favoring the octahedrally coordinated 1T- MoS_2 . The NH_4^+ ion destabilizes the trigonal-prismatic 2H- MoS_2 structure and favors the octahedrally coordinated 1T- MoS_2 .

The microwave irradiation has two effects on the synthesis of 1T/2H-MoS₂. First, the microwave dipole rotation destroys the weak van der Waals forces between the MoS₂ layers and increases their interlayer spacing (shift (002) peaks to lower angel in XRD patterns). Second, ammonium ions enter the MoS₂ interlayers in a non-uniform manner, making the lattice unstable for phase transition from 2H to 1T. As previously stated, there are three groups (d_{xz}, d_{yz}) , $(d_{xy}, d_{x^2y^2})$, and (d_{z^2}) of electrons in the 4d orbital of Mo in the 2H phase, of which the (d_{z^2}) orbital is filled with electrons, leaving other orbitals empty and contributing to the phase structure's stability (Figure 6). After being exposed to microwave radiation, the ammonium ions in the matrix cause an electron to partially occupy the $(d_{xy}, d_{x^2y^2})$ orbital, reducing its stability and facilitating phase conversion from the 2H to the 1T phase. The electrons of Mo are occupied in two of the three degenerate orbitals in the two groups $(d_{x^2y^2}, d_{z^2})$ and (d_{xy}, d_{xz}, d_{yz}) of the 1T phase (d_{xy}, d_{xz}, d_{yz}) . As a result of the three degenerate orbitals being filled, the addition of an electron increases phase stability. Because of lattice instability, the interaction between MoS₂ and ammonium ions weakens the top Mo–S bond, causing phase conversion from the 2H to 1T phase [29].



(B)

Figure 6. (A) 2H-MoS₂ crystal structure and ligand splitting for 4d orbitals of Mo atoms with trigonal-prismatic coordination, (B) 1T-MoS₂ crystal structure and ligand splitting for 4d orbitals of Mo atoms with octahedral coordination.

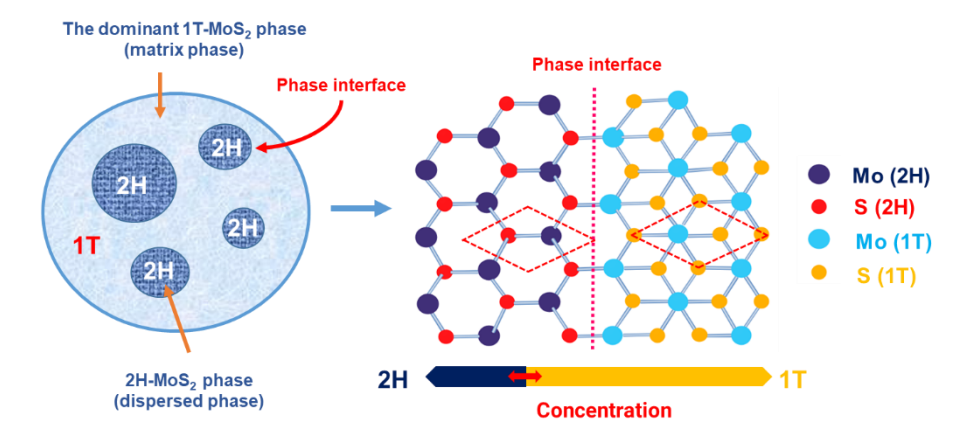


Figure 7. An illustration of the phase distribution in a 1T/2H-MoS₂ material where 1T is the dominant phase.

The hybrid materials in S1-EG, S2-EG+G, S3-G demonstrate that the 1T phase has a more dominating composition than the 2H phase, based on the results of computing the 1T and 2H phase compositions using XPS spectra. As a result, we refer to the phase that occupies the upper component as the matrix phase and the remaining phase as the randomly dispersed phase inside the matrix phase. Figure 7 illustrates the phase distribution of the 1T and 2H phases in the synthesized MoS_2 hybrid material.

4. CONCLUSIONS

In conclusion, the successful synthesis of 1T/2H-MoS₂ nanomaterials using a green method based on microwave heating and green solvent polyols has been demonstrated. This new approach offers several advantages over conventional synthesis methods, including shorter reaction times, lower energy consumption, and the use of environmentally friendly solvents. The use of polyol solvents including ethylene glycol (EG), ethylene glycol mixed with glycerol (G) in a volume ratio of 1:1, and glycerol (G) has been shown to be effective in controlling the phase fraction of 1T/2H MoS₂, with the highest 1T concentration reaching 84.5 %. This is a significant achievement, as the 1T phase has been shown to exhibit superior electrochemical performance due electrical enhanced conductivity. The reaction mechanism and phase transition between the 1T and 2H phases have been described and illustrated, shedding light on the complex behavior of this hybrid material. The role of polyol solvents in the practical synthesis of nano MoS₂ under microwave heating has also been evaluated and explained.

Acknowledgements. We acknowledge Ho Chi Minh City University of Technology (HCMUT), VNU-HCM for supporting this study.

CRediT authorship contribution statement. Vinh-Dat Vuong: Methodology and Investigation; Minh Nguyet Nguyen: Data curation, Conceptualization, Writing - original draft; Nguyen Huu Huy Phuc, Thang Van Le: Reviewing and Supervision.

Declaration of competing interest. The authors declare that they have no known competing financial interests or personal relationships that could have appeared to influence the work reported in this paper.

REFERENCES

- 1. Wang D., Zhang X., Bao S., Zhang Z., Fei H., and Wu Z. Phase engineering of a multiphasic 1T/2H MoS₂ catalyst for highly efficient hydrogen evolution, J. Mater. Chem. A **9** (6) (2017) 2681-2688. https://doi.org/10.1039/C6TA09409K.
- 2. Tang Q. and Jiang D. E. Mechanism of Hydrogen Evolution Reaction on 1T-MoS₂ from First Principles, ACS Catal. **6** (8) (2016) 4953-4961. https://doi.org/10.1021/acscatal.6b01211
- 3. Damien Voiry M. S., Silva R., Fujita T., Chen M., Asefa T., Shenoy Vivek B., Eda G., and Chhowalla M. Conducting MoS₂ nanosheets as catalysts for hydrogen evolution reaction, Nano Lett. **13** (12) (2013) 6222-6227. https://doi.org/10.1021/nl403661s
- Yang J., Wang K., Zhu J., Zhang C., and Liu T. Self-Templated Growth of Vertically Aligned 2H-1T MoS₂ for Efficient Electrocatalytic Hydrogen Evolution, ACS Appl. Mater. Interfaces. 8 (46) (2016) 31702-31708. https://doi.org/10.1021/acsami.6b11298
- 5. Zhou Y. *et al.* Rational design and synthesis of 3D MoS2 hierarchitecture with tunable nanosheets and 2H/1T phase within graphene for superior lithium storage, Electrochim. Acta. **211** (2016)1048-1055. https://doi.org/10.1016/j.electacta.2016.06.123
- 6. Wu M. *et al.* Metallic 1T MoS₂ nanosheet arrays vertically grown on activated carbon fiber cloth for enhanced Li-ion storage performance, J. Mater. Chem. A **5** (27) (2017) 14061-14069. https://doi.org/10.1039/C7TA03497K
- 7. Wang D., Xiao Y., Luo X., Z. Wu, Wang Y.-J., and Fang B. Swollen Ammoniated MoS_2 with 1T/2H Hybrid Phases for High-Rate Electrochemical Energy Storage, ACS Sustain Chem Eng., **5** (3) (2017) 2509-2515. https://doi.org/10.1021/acssuschemeng.6b02863
- 8. Jiang L. *et al.* Optimizing Hybridization of 1T and 2H Phases in MoS₂ Monolayers to Improve Capacitances of Supercapacitors, Mater. Res. Lett. **3** (4) (2015) 177-183. https://doi.org/10.1080/21663831.2015.1057654
- 9. Huang H. *et al.* Metallic 1T phase MoS₂ nanosheets for high-performance thermoelectric energy harvesting, Nano Energy **26** (2016) 172-179. https://doi.org/10.1016/j.nanoen.2016.05.022
- 10. Hsiao M. C. *et al.* Ultrathin 1T-phase MoS₂ nanosheets decorated hollow carbon microspheres as highly efficient catalysts for solar energy harvesting and storage, J. Power Sources **345** (2017) 156-164. https://doi.org/10.1016/j.jpowsour.2017.01.132
- 11. Gigot A. *et al.* Mixed 1T–2H Phase MoS₂/Reduced Graphene Oxide as Active Electrode for Enhanced Supercapacitive Performance, ACS Appl. Mater. Interfaces., **8** (48) (2016) 32842-32852. https://doi.org/10.1021/acsami.6b11290

- 12. Zhang Y., Kuwahara Y., Mori K., Louis C., and Yamashita H., Hybrid phase 1T/2H-MoS₂ with controllable 1T concentration and its promoted hydrogen evolution reaction, Nanoscale **12** (22) (2020) 11908-11915. https://doi.org/10.1039/D0NR02525A
- 13. Geng X. *et al.* Pure and stable metallic phase molybdenum disulfide nanosheets for hydrogen evolution reaction, Nat. Commun. **7** (1) (2016) 10672. https://doi.org/10.1038/ncomms10672
- 14. Lei Z., Zhan J., Tang L., Zhang Y., and Wang Y. Recent Development of Metallic (1T) Phase of Molybdenum Disulfide for Energy Conversion and Storage, Adv. Energy Mater. 8 (19) 1703482 (2018). https://doi.org/10.1002/aenm.201703482
- 15. Liu Q. *et al.* Gram-Scale Aqueous Synthesis of Stable Few-Layered 1T-MoS₂: Applications for Visible-Light-Driven Photocatalytic Hydrogen Evolution, Small**11** (41) (2015) 5556-5564. https://doi.org/10.1002/smll.201501822
- 16. Chen Y.X., Wu C.W., Kuo T.Y., Chang Y.L., Jen M.H., and Chen I. W. P. Large-Scale Production of Large-Size Atomically Thin Semiconducting Molybdenum Dichalcogenide Sheets in Water and Its Application for Supercapacitor, Sci. Rep. 6 (1) (2016)26660. https://doi.org/10.1038/srep26660
- 17. Ali M. E. M., Mohammed R., Abdel-Moniem S. M., El-Liethy M. A., and Ibrahim H. S. Green MoS₂ nanosheets as a promising material for decontamination of hexavalent chromium, pharmaceuticals, and microbial pathogen disinfection: spectroscopic study, J Nanopart Res. **24** (10) (2022). https://doi.org/10.1007/s11051-022-05573-6
- 18. Pallikkarathodi Mani N. and Cyriac J. Green approach to synthesize various MoS₂ nanoparticles via hydrothermal process, Bull. Mater. Sci.,**45** (4) (2022). https://doi.org/10.1007/s12034-022-02757-7
- 19. Madani M. *et al.* Green synthesis of nanoparticles for varied applications: Green renewable resources and energy-efficient synthetic routes, Nanotechnol. Rev.**11** (1) (2022) 731-759. https://doi.org/10.1515/ntrev-2022-0034
- 20. Priecel P. and Lopez-Sanchez J. A. Advantages and Limitations of Microwave Reactors: From Chemical Synthesis to the Catalytic Valorization of Biobased Chemicals, ACS Sustain Chem Eng. 7 (1) (2019) 3-21. https://doi.org/10.1021/acssuschemeng.8b03286
- 21. Dong H., Chen Y. C., and Feldmann C. Polyol synthesis of nanoparticles: status and options regarding metals, oxides, chalcogenides, and non-metal elements, Curr. Green Chem. 17 (8) (2015) 4107-4132. https://doi.org/10.1039/C5GC00943J
- 22. Collins T. J. Review of the twenty-three year evolution of the first university course in green chemistry: teaching future leaders how to create sustainable societies, J. Clean. Prod.**140** (2017)93-110. https://doi.org/10.1016/j.jclepro.2015.06.136
- 23. Castillo-Henriquez L., Alfaro-Aguilar K., Ugalde-Alvarez J., Vega-Fernandez L., Montes de Oca-Vasquez G., and Vega-Baudrit J. R. Green Synthesis of Gold and Silver Nanoparticles from Plant Extracts and Their Possible Applications as Antimicrobial Agents in the Agricultural Area, Nanomaterials (Basel) 10 (9) (2020). https://doi.org/10.3390/nano10091763
- 24. Waskito I. S., Kurniawan B., Amal M. I., and Hanifuddin M. The Effect of Precursors Concentration on the Structural Properties of MoS₂ Nanosheet-Microsphere Synthesized Via Hydrothermal Route, IOP Conf. Ser. Mater. Sci. Eng.**546** (2019). http://dx.doi.org/10.1088/1757-899X/546/4/042048

- 25. Wang F., Li G., Zheng J., Ma J., Yang C., and Wang Q. Hydrothermal synthesis of flower-like molybdenum disulfide microspheres and their application in electrochemical supercapacitors, RSC Adv.8 (68) 92018) 38945-38954. https://doi.org/10.1039/C8RA04350G
- 26. Suo Xia Hou C. W., Jie Huo Y. Controllable Preparation of Nano Molybdenum Disulfide by Hydrothermal Method, Ceram. Silik.,**61** (2) (2017) 158 162, 2017. https://doi.org/10.13168/cs.2017.0011
- 27. Saber M., Khabiri G., Khabiri A. M., Ulbricht M., Khalil A., and M. R A comparative study on the photocatalytic degradation of organic dyes using hybridized 1T/2H, 1T/3R and 2H MoS₂ nano-sheets, RSC Adv.**8** (2018)26364-26370. https://doi.org/10.1039/C8RA05387A
- 28. Saseendran S. B., Ashok A., and A. A S Edge terminated and interlayer expanded pristine MoS₂ nanostructures with 1T on 2H phase, for enhanced hydrogen evolution reaction, Int. J. Hydrogen Energy.**47** (16) (2022) 9579-9592. https://doi.org/10.1016/j.iihydene.2022.01.031
- 29. Das S., Swain G., and Parida K. One step towards the 1T/2H-MoS₂ mixed phase: a journey from synthesis to application, Mater. Chem. Front.**5** (5) (2021) 2143-2172. https://doi.org/10.1039/D0QM00802H
- 30. Das S., Swain G., and Parida K. One step towards the 1T/2H-MoS₂ mixed phase: a journey from synthesis to application, Mater. Chem. Front.**5** (5) (2021) 2143-2172. https://doi.org/10.1039/D0QM00802H
- 31. Wang H. W., Skeldon P., and Thompson G. E. XPS studies of MoS_2 formation from ammonium tetrathiomolybdate solutions, Surf. Coat. Int.**91** (3) (1997) 200-207. https://doi.org/10.1016/S0257-8972(96)03186-6
- 32. John F. Moulde W. F. S., Peter E. S., Kenneth Bomben D. Handbook of X-ray photoelectron spectroscopy, 1992
- 33. Cheng P., Sun K., and Hu Y. H. Memristive Behavior and Ideal Memristor of 1T Phase MoS₂ Nanosheets, Nano Lett.**16** (1) (2016) 572-576. https://doi.org/10.1021/acs.nanolett.5b04260
- 34. Hou M. et al. Aging mechanism of MoS_2 nanosheets confined in N-doped mesoporous carbon spheres for sodium-ion batteries, Nano Energy**62** (2019) 299-309. https://doi.org/10.1016/j.nanoen.2019.05.048
- 35. Gao X., Xiong L., Wu J., Wan J., and Huang L. Scalable and controllable synthesis of 2D high-proportion 1T-phase MoS₂, Nano Research**13** (11) (2020) 2933-2938. https://doi.org/10.1007/s12274-020-2950-2
- 36. Xin X. *et al.* In-situ growth of high-content 1T phase MoS₂ confined in the CuS nanoframe for efficient photocatalytic hydrogen evolution, Appl. Catal. B: Enviro.**269** (2020) 118773. https://doi.org/10.1016/j.apcatb.2020.118773
- 37. Feng D., Pan X., Xia Q., Qin J., Zhang Y., and Chen X. Metallic MoS_2 nanosphere electrode for aqueous symmetric supercapacitors with high energy and power densities, J. Mater. Sci.55 (2020) 1-11. https://doi.org/10.1007/s10853-019-03997-5
- 38. Yu Y. *et al.* High phase purity 1T'-MoS2 and 1T'-MoSe2 layered crystals, Nat. Chem.**10** (6) (2018) 638-643. https://doi.org/10.1038/s41557-018-0035-6

- 39. Wei J. *et al.* Synthesis of Few Layer Amorphous 1T/2H MoS₂ by a One-Step Ethanol/Water Solvothermal Method and Its Hydrodesulfurization Performance, Catal. Letters**152** (1) (2021) 263-275. https://doi.org/10.1007/s10562-021-03621-9
- 40. Wang S., Luo Y., Fan Y., Ali A., Liu Z., and Kang Shen P. Uniformly distributed 1T/2H-MoS₂ nanosheets integrated by melamine foam-templated 3D graphene aerogels as efficient polysulfides trappers and catalysts in lithium-sulfur batteries, J. Electroanal.Chem.**909** (2022). https://doi.org/10.1016/j.jelechem.2022.116099
- 41. Agrawal A. V. et al. Controlled Growth of MoS₂ Flakes from in-Plane to Edge-Enriched 3D Network and Their Surface-Energy Studies, ACS Appl. Nano Mater.1 (5) (2018) 2356-2367. https://doi.org/10.1021/acsanm.8b00467
- 42. Kim J. S. *et al.* Electrical Transport Properties of Polymorphic MoS₂, ACS Nano,**10** (8) (2016 7500-7506. https://doi.org/10.1021/acsnano.6b02267
- 43. Lee Y. B. et al. Facile microwave assisted synthesis of vastly edge exposed 1T/2H-MoS₂ with enhanced activity for hydrogen evolution catalysis, J. Mater. Chem.**7** (8) (2013) 3563-3569. https://doi.org/10.1039/C8TA12080C
- 44. Cai L. *et al.* High-Content Metallic 1T Phase in MoS₂-Based Electrocatalyst for Efficient Hydrogen Evolution, J. Phys. Chem. C121 (28) (2017) 15071-15077, https://doi.org/10.1021/acs.jpcc.7b03103
- 45. Guo X., Wang Z., Zhu W., and Yang H. The novel and facile preparation of multilayer MoS2 crystals by a chelation-assisted sol–gel method and their electrochemical performance, RSC Adv. 7 (15) (2017) 9009-901. https://doi.org/10.1039/C6RA25558B
- 46. Wojnarowicz J. et al. Effect of Water Content in Ethylene Glycol Solvent on the Size of ZnO Nanoparticles Prepared Using Microwave Solvothermal Synthesis, J. Nanomater. **2016** (2016) 1-15. https://doi.org/10.1155/2016/2789871
- 47. Zheng Y. et al. The effect of lithium adsorption on the formation of 1T-MoS2 phase based on first-principles calculation, Phys. Lett. A **380** (20) (2016) 1767-1771. https://doi.org/10.1016/j.physleta.2016.03.009